Grant Agreement number: 773421

H2020-BG-2016-2017/H2020-BG-2017-1

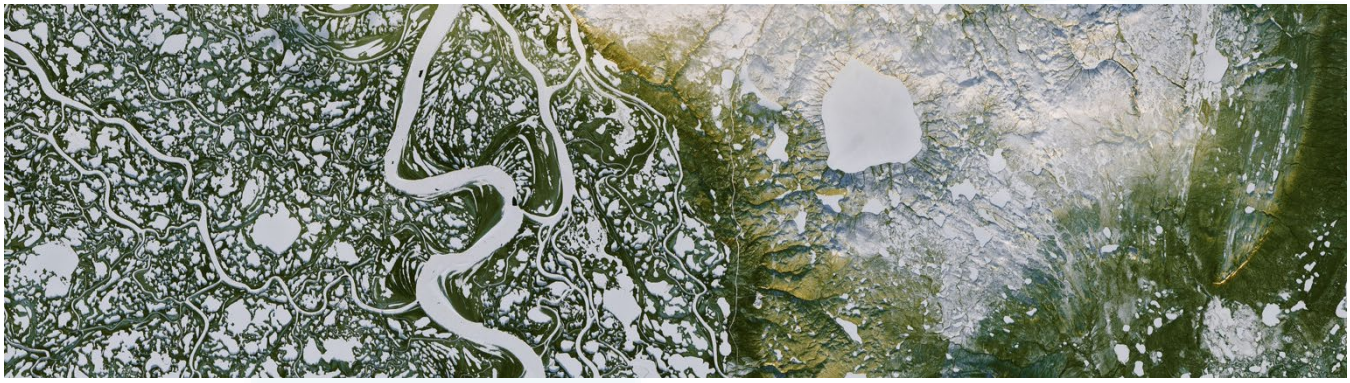

Deliverable Report

Work package	WP6
Deliverable No. (DX.X) - Title	Report on Field Investigation and Long-Term Plate Loading test in Permafrost
Lead Beneficiary (acronym)	NTNU/DTU
Authors (Name, Institution)	Seyed Ali Ghoreishian Amiri, NTNU
Editors (Name, Institution)	Knut Vilhelm Høyland, NTNU
Contributors (Name, Institution)	Chuangxin Lyu, NTNU; Aleksey Shestov, UNIS; Arne Aalberg, UNIS-NTNU; Gustav Grimstad, NTNU; Gudmund Reidar Eiksund, NTNU
Status	☒ Draft ☐ WP manager accepted ☐ Project coordinator accepted
Nature	R
Dissemination level	☒ PU - Public ☐ PP - Restricted to programme participants ☐ RE - Restricted to a group specified by the consortium ☐ CO - Confidential, only for members of the Consortium
Submission Date	31/10/2023

Summary

This report presents a comprehensive overview of field investigations and large-scale plate loading tests conducted at the UNIS East site in Longyearbyen from March 2020 to July 2023. These tests were undertaken as part of the NUNATARYUK project, with a primary focus on studying the long-term behaviour of frozen soil in response to temperature change and permafrost degradation. The significance of this study and report lies in their contribution to the assessment of climate change impacts on permafrost regions, particularly with respect to infrastructure stability.

The design of the long-term plate loading test was based on a systematic site investigation carried out under the NGTS (Norwegian Geo-Test Sites) project. The design encompassed natural permafrost sampling, laboratory testing, back calculation of test results, and the establishment of a meticulously organized setup for continuous long-term monitoring and data collection.

The test conducted at Longyearbyen, Norway, where the ground in a large part of the city is Holocene marine deposits. The active layer thickness in the region was approximately 1 to 2 meters. Sampling was conducted at depths of 4 to 6 meters in boreholes located approximately 1 meter from the plate loading test site. Three footing plates, with 300 mm diameter each, were placed on saline clay permafrost at around 4.2 m depth. An equilateral triangle steel frame with an edge length around 4 m is supported by these three legs and used for a loading platform though adding concrete blocks as dead weight. A stepwise loading procedure was adapted to monitor the long-term creep settlements.

The experimental results and field measurements reveal that the mechanical implications of a warming climate extend beyond the typical melting point, impacting the frozen soil several degrees below that temperature. Ground subsidence initiates through a creep deformation in the warming frozen soil, several degrees below the melting point, which is then followed by an accelerated deformity caused by thawing settlement as temperatures approach the melting point. The observations suggest that creep deformation may contribute significantly to the overall subsidence phenomenon.

In addition to the direct insights gained from these tests regarding the long-term behaviour of frozen soil in response to temperature changes, it’s imperative to highlight its significance as benchmark problem for verifying and refining computational models and simulations. The data and observations collected during this extensive study provide valuable reference points for developing and testing predictive models. Such models are essential for assessing the impacts of climate change on permafrost regions and their associated infrastructures.

Table of Contents

1 Introduction

Over the past half-century, there has been clear evidence of global-scale permafrost warming and degradation driven by climate change (Aalto et al., 2018; Biskaborn et al., 2019; Osterkamp, 2007; Wu and Zhang, 2008). This ongoing process has raised substantial concerns regarding infrastructure damage and threats to human safety associated with permafrost degradation (*Doré et al.*, 2016; *Duvillard et al.*, 2019). In areas where stable permafrost was previously assumed during construction, these changes present significant geotechnical challenges and create demanding conditions. The problem is already highlighted in the news, e.g. (*Karijord*, 2018; *Luhn*, 2016; *OSBORNE*, 2018), reporting a growing problem of cracking and collapsing buildings in Russia, Canada, Alaska and Svalbard.

Frozen soil in permafrost regions is a natural composite consisting of solid grains, ice, unfrozen water, and air. Temperature variations cause (at least part of) the pore water to freeze and thaw, even at temperatures below the typical melting point. These variations involve complex coupled thermal, hydraulic and mechanical processes. The phase change caused by temperature variation will, for example, affect the hydraulic regime of the medium, which in turn induces mechanical deformation. Understanding these mechanical deformations is crucial for designing safe construction practices and predicting potential hazards in engineering activities within cold regions and artificial ground freezing. The temperature dependent behaviour of frozen soil is of fundamental importance in this understanding and evaluation.

Experimental results and field measurements demonstrate that creep deformation in frozen soil is significantly influenced by temperature and ice content (*Eckardt*, 1979; *Ghoreishian Amiri et al.*, 2022). The creep properties of frozen soil are primarily associated with the ice phase, with ice exhibiting more viscous behaviour at higher temperatures. Consequently, the rate of creep deformation increases in frozen soils with higher ice content and temperature.

In Svalbard, the annual average temperature has increased by 3-5°C during the last 40 years. The frozen marine deposits in Svalbard, particularly saline clay and silt found widely in the fjord-valleys, are highly susceptible to creep under this warming period. To investigate this phenomenon and establish a benchmark test for further analytical and numerical analysis of frozen soil, a plate test frame has been installed at the layer of marine permafrost. The frame is loaded with dead weights and meticulously monitored for foundation settlement and ground temperature changes over time. The legs are specifically designed to resist external loading only at the foot.

This footing test is a component of the Nunataryuk project, funded by the European Union's Horizon 2020 Research and Innovation Program (https://nunataryuk.org/). Nunataryuk's primary objective is to assess the impacts of thawing land, coast, and subsea permafrost on Arctic communities. The project also aims to develop tailored, co-designed adaptation, and mitigation strategies.

2 Site background

Longyearbyen, the largest settlement on Svalbard with around 2000 residents, hosts numerous students and researchers, contributing to increased human activity. Much of its infrastructure is built on permafrost, making it vulnerable to permafrost degradation. The town's growing housing needs require sustainable construction, particularly in light of climate change and permafrost degradation.

Since 1980, Longyearbyen has experienced a significant temperature increase, with a 0.72°C rise in the 30-year average air temperature per decade (*Instanes*, 2016). Projections indicate that by 2100, annual average temperatures could surge by 4-6°C, with winter temperatures expected to rise by around 10°C (*Etzelmüller et al.*, 2011). These increases will trigger permafrost degradation in the region.

The Norwegian Geo-Test Sites (NGTS) project conducted thoroughly engineering geology assessment and further developed two geotechnical field test sites: Adventdalen and UNIS East (Fig. 1-A), for permafrost study in Longyearbyen (Gilbert et al., 2019). The UNIS East site is closed to the Svalbard Science Centre (Fig. 1-B) and inside the town of Longyearbyen, selected for the long-term plate loading experiment.

The site investigation reveals consistent salinity, water content, and grain size distribution in the marine permafrost, with minor variations. Besides, it also suggests that core sampling can be performed at shallow depth (e.g. 4~6 m), and experimental results can generally represent physical and mechanical properties of whole frozen layer.

Gilbert et al. (2019) reports electrical resistivity tomography of UNIS East site. In the tested site, boreholes were made down to 30 m, and several temperature stings were installed to measure temperature profile with time starting from 2017. Besides, the soil stratigraphy at the site consists of a 3 m sandy layer above 30 m of marine saline silty clay overlying the bedrock.

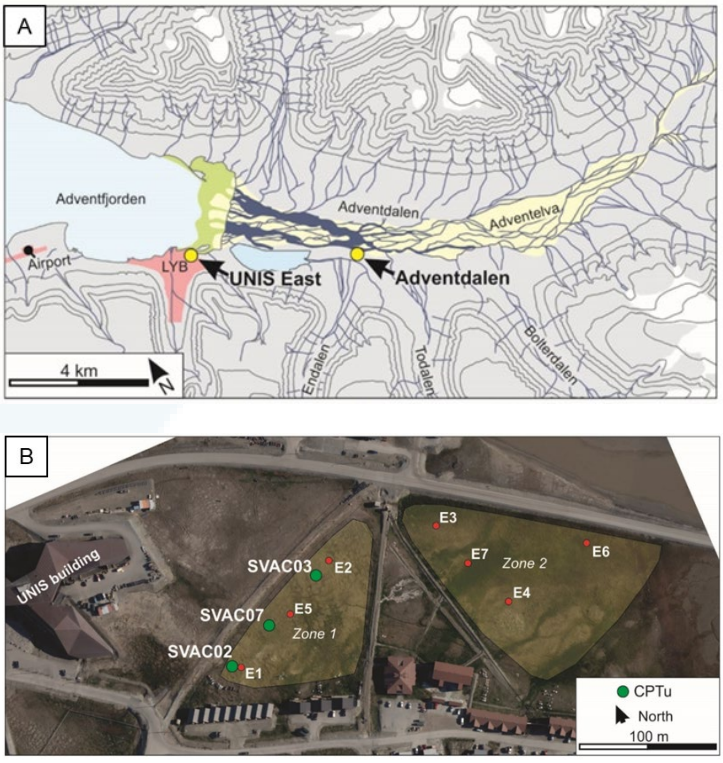

Fig. 1 A) Location of the Adventdalen and UNIS East sites in the town of Longyearbyen (LYB); B) Details of the UNIS East site (Gilbert et al., 2019)

3 Natural sample collection

The sampling was performed at a depth of 4-6 meters from two boreholes, located approximately 1 meter from the plate loading test site. Down-the-hole (DTH) drilling was employed, reaching a depth of 3.5 meters. Bag samples of drilling cuts were collected during drilling. Since the active layer was frozen during the winter, no casing was required to maintain the boreholes.

To retrieve intact samples, the DTH drilling rig was replaced with a SINTEF-modified CRREL coring auger (Fig. 2) with a 45 mm diameter and 400mm length. This specialized corer featured cutting bits attached to a thick-walled

hollow stem auger. A hydraulic-pumped extruder (Fig. 3-A) was used to push the sampling core out of the stem auger. Subsequently, the cores were cut into 80-90 mm lengths at the cold lab at UNIS (Fig. 3-B).

The processed samples were then placed in two pre-cooled thermal-insulated boxes, containing frozen eutectic packs with a phase change temperature of -3°C. These samples were transported for 24 hours to the geotechnical lab at the Norwegian University of Science and Technology (NTNU). They were stored in a cold room with a constant temperature of -3°C, close to the in-situ ground temperature. All measures were taken to minimize thermal disturbance. X-ray scanning (Fig. 3-C) confirmed that the samples remained undisturbed during the coring and transportation process, although some cryo-structures were observed in a few natural samples.

Approximately 20 samples were collected and transported back to NTNU for laboratory testing. The primary focus was on assessing their mechanical behaviour and unfrozen water saturation. As a result, a total number of twelve triaxial creep tests were conducted on these samples, subjecting them to various temperature and deviatoric stress conditions. Additionally, electrical resistivity tests were carried out on four samples to monitor their behaviour during freezing and thawing. For further insights, three samples underwent X-ray scanning. The remaining three samples, along with post-tested ones, were used to prepare remoulded samples for thermal conductivity measurements.

Fig. 2 SINTEF-modified CRREL coring auger (Gilbert et al., 2019)

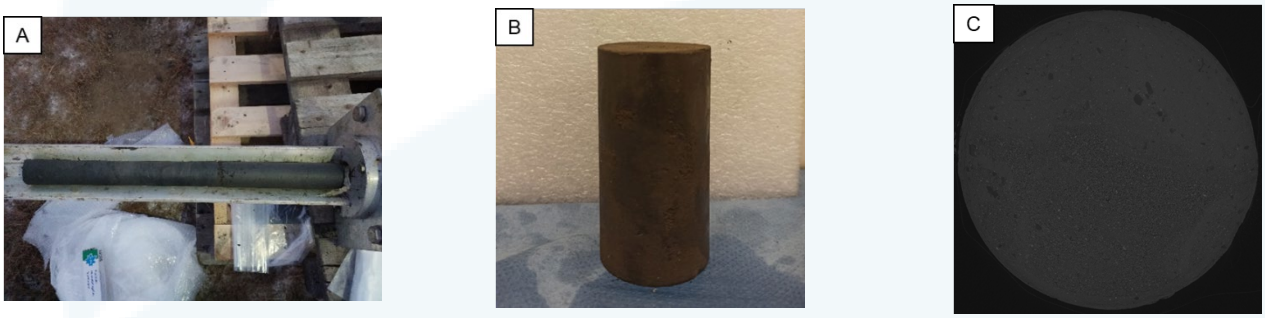

Fig. 3 A) The sampling cores; B) The processed sample with 80~90 mm in length; C) X-ray scanning of natural samples (*Lyu*, 2021)

4 Laboratory investigation

4.1 Measurement of unfrozen water content

The Electrical Resistivity (ER) tests were conducted on undisturbed natural permafrost samples to estimate the unfrozen water content (UWC) over a temperature range of -17°C to 1°C. The ER testing setup (depicted in Fig. 4-A) involved a voltage signal generator (NI 9269) and a voltage recording module (NI 9205). To pass the current through the samples, two stainless steel electrode meshes were affixed at either end. Additionally, two stainless steel pin electrodes, featuring PT100 sensors at their tips to monitor internal sample temperature, were inserted into the samples at a separation of 30 mm to measure the potential drop.

For precise current flow measurement, a shunt resistor box with resistance values ranging from 50 to 10,000 Ohms was placed in series with the sample. To maintain undisturbed conditions, the samples were covered with plastic wrapping to prevent sublimation and stored in a temperature-controlled freezer at -3°C. To reduce contact resistance, the pin electrodes were wetted with saline water before insertion.

Before conducting soil testing, the experimental setup was validated by measuring the resistivity of saline water at various salt concentrations (ranging from 20 to 40 g/L) and the results were compared with values obtained using an electrical conductivity meter.

Fig. 4-B illustrates a square wave voltage signal with a 4-second period and the potentials measured over the shunt resistor box and the sample. At each signal reversal, there is an initial spike followed by a decay, which is attributed to induced polarization in the sample. The measured voltage signal has relaxed to stable values after 0.6 to 0.8 s, and voltages recorded after an initial delay of 1.8 s in each excitation were used to estimate the apparent resistivity of the sample (ρ).

Testing began at -3°C, which approximates the in-situ ground temperature at a depth of 4 to 6 meters. The temperature was then gradually decreased by 1 to 3°C in each step, ultimately reaching -17°C. The ρ was measured when the samples reached thermal equilibrium in each step, minimizing the impact of temperature variations within the samples. Finally, the tested samples were warmed above thawing temperature to measure the ρ of unfrozen samples.

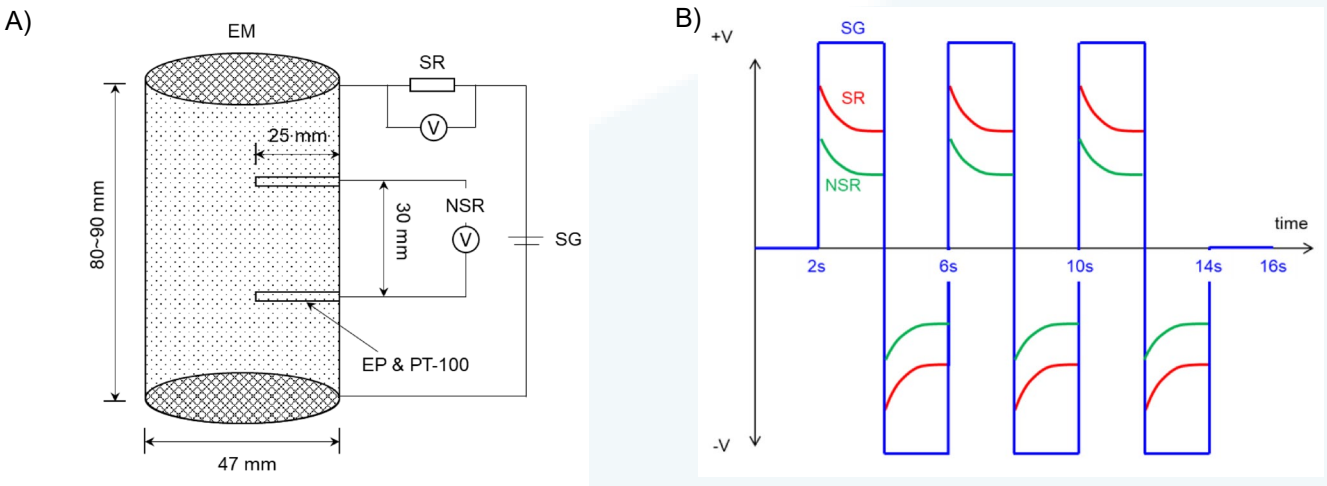

Fig. 4 Electrical resistivity measurement (Lyu, 2021): A) Sketch of the test setup. Note: EM (electrode mesh), SR (shunt resistance), NSR (natural sample resistance), SG (signal generator as input signal), V (voltage recording module) and EP & PT-100 (pin electrodes and PT-100 sensor); B) Schematic illustration of signal generator as input signal (SG) and output signal (electrical potential cross SR and EPs)

4.1.1 Test results

Electrical resistivity tests were conducted on four natural samples, denoted as specimens S1 to S4, extracted from soil depths ranging from 4.6 meters to 5.8 meters. Fig. 5-A depict the variation in apparent electrical resistivity (ρ) concerning temperature (T) for each of the tests. Notably, ρ exhibits a significant increase, ranging from approximately 2 Ωm in the unfrozen state to about 100 Ωm at T = -17°C due to its dependency on UWC. Additionally, the figures include data on gravimetric water content and salinity.

Archie's law has been employed to establish a correlation between unfrozen water saturation, denoted as Sw and defined as the ratio of unfrozen water content (UWC) to the total water content in fully saturated marine clay, and the apparent electrical resistivity (ρ) for partially frozen soils.

Archie's law was thus adopted to correlate unfrozen water saturation (UWS), S_w, defined as the ratio of UWC to total water content for fully saturated marine clay, with ρ for partially frozen soils (*Oldenborger and LeBlanc*, 2018):

$$\rho_\alpha = a(\rho_w)_\alpha \phi^{-m} S_w^{-n} \quad ; \quad \alpha = u, f \tag{1}$$

where u and f refer to unfrozen and frozen states, respectively, ρ_w is the pore water resistivity which depends on salinity and temperature, a, m and n are empirical constants, and ϕ is the porosity. S_w is then derived as:

$$S_w = \left(\frac{(\rho_w)_f}{(\rho_w)_u} \frac{\rho_u}{\rho_f} \right) \tag{2}$$

ρ_u and ρ_f are measured for undisturbed natural permafrost samples as a function of temperature. The resistivity of the unfrozen water at sub-zero temperature $(\rho_w)_f$ is expected to decrease with decreasing temperature as ions are expelled to the unfrozen water from the gradually forming ice matrix (*Lyu et al.*, 2020). The increasing ion concentration results in a decrease in ρ_w, which has been considered by *Lyu* (2021):

$$(\rho_w)_f = S_w.(\rho_w)_u \tag{3}$$

As the temperature decreases, ionic mobility also decreases and further ρ_w increases. The temperature dependency has been measured and correlated above 0°C (*Keller and Frischknecht, 1966*), while *Oldenborger and LeBlanc* (2018) used NaCl solutions to measure saline water resistivity variation at subzero temperature. The latter proposed a quadratic equation including empirical constants $a = 0.021$ °C^{-1} and $b = 8.68 \times 10^{-5}$ °C^{-2} with around 1% prediction error:

$$\rho_w = \frac{(\rho_w)_R}{\left[1 + a(T - T_R) + b(T - T_R)^2\right]} \tag{4}$$

where $(\rho_w)_R$ is the water resistivity at the reference temperature T_R. By combining equation (2), (3) and (4), the following equation is used for the unfrozen water saturation estimate ($S_w = 1$ means saturated unfrozen soil):

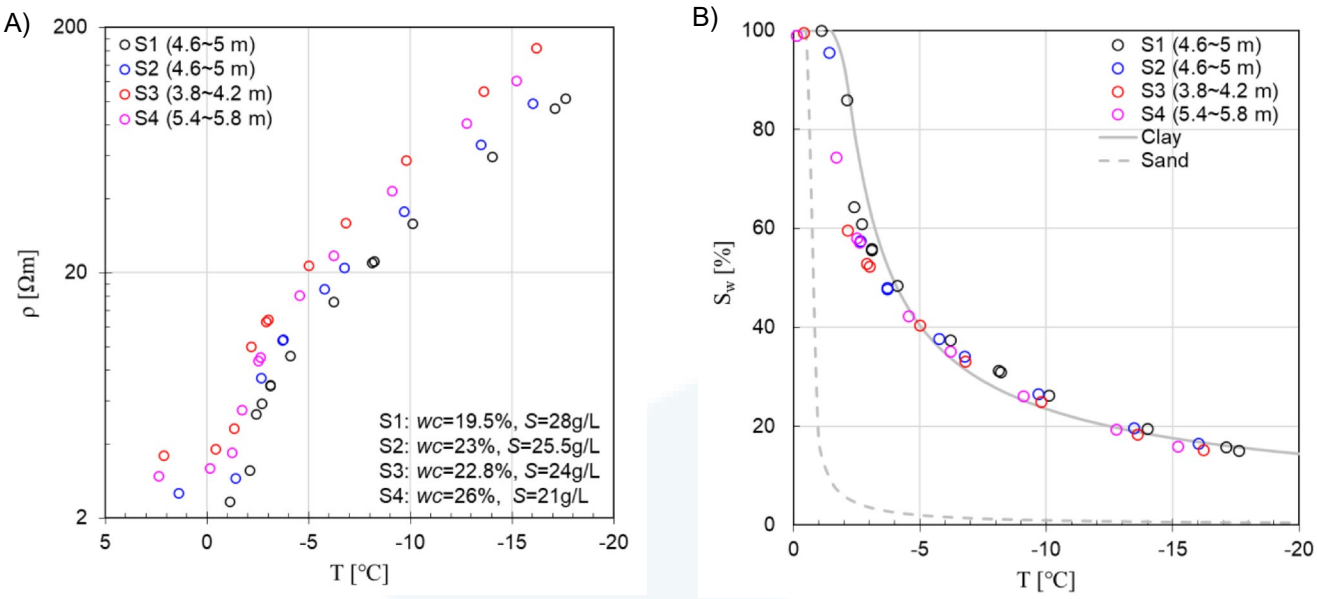

Fig. 5 ER test results for natural saline marine permafrost and estimated Sw curve based on Archie's law (Lyu, 2021); A) ρ vs. T for S1~S4 samples; B) UWS (Sw) vs. T for natural samples and numerical simulation. (Note: The UWS curve for sandy layer is deduced by the information that it is non-saline coarse-grained soil with around -0.5 ℃ freezing point according to NGTS report

$$S_w = \left(\frac{\rho_u}{\left[1 + a\left(T_f - T_u\right) + b\left(T_f - T_u\right)^2\right]\rho_f} \right)^{\frac{1}{n-1}} \tag{5}$$

where T_f and T_u refer to the tested temperatures at which ρ_f and ρ_u are measured in frozen and unfrozen state respectively. The factor n varies with the soil type and properties. By considering the soil type and reported UWS curves of similar saline clay, *Lyu et al.* (2020) concluded that $n = 2$ is a reasonable value for the selected test site. The final result is presented in Fig. 5-B.

4.2 Measurement of thermal conductivity

The thermal conductivity (k_T) of the permafrost was determined using a steady-state method, as illustrated in Fig. 6-A. This setup closely resembled the one employed by Côté and Konrad (2005). Units provided the heat flow, and the entire system was insulated. The known thermal conductivity of borosilicate glass (1.04 W/(mK)) combined with the measured temperature difference across the glass disc allowed for calculation of the heat flux through the soil sample.

For the thermal conductivity tests, it was necessary to remould the natural soil to match the diameter of the glass discs. This process involved drying and grinding the soil, followed by compaction in a plexiglass mould with a sealed aluminium bottom. This was carried out to achieve a dry density comparable to that of the natural frozen soil. The compacted dry soil was then mixed with distilled water to replicate the gravimetric water content of the natural soil (*wc*=23%), and allowed to settle for 24 hours to ensure even water distribution. Pore fluid was extracted and measured using an electrical conductivity meter, revealing a salinity value (S) of 20 g/L. The thermal conductivity (k_T) of the sample was determined as follows:

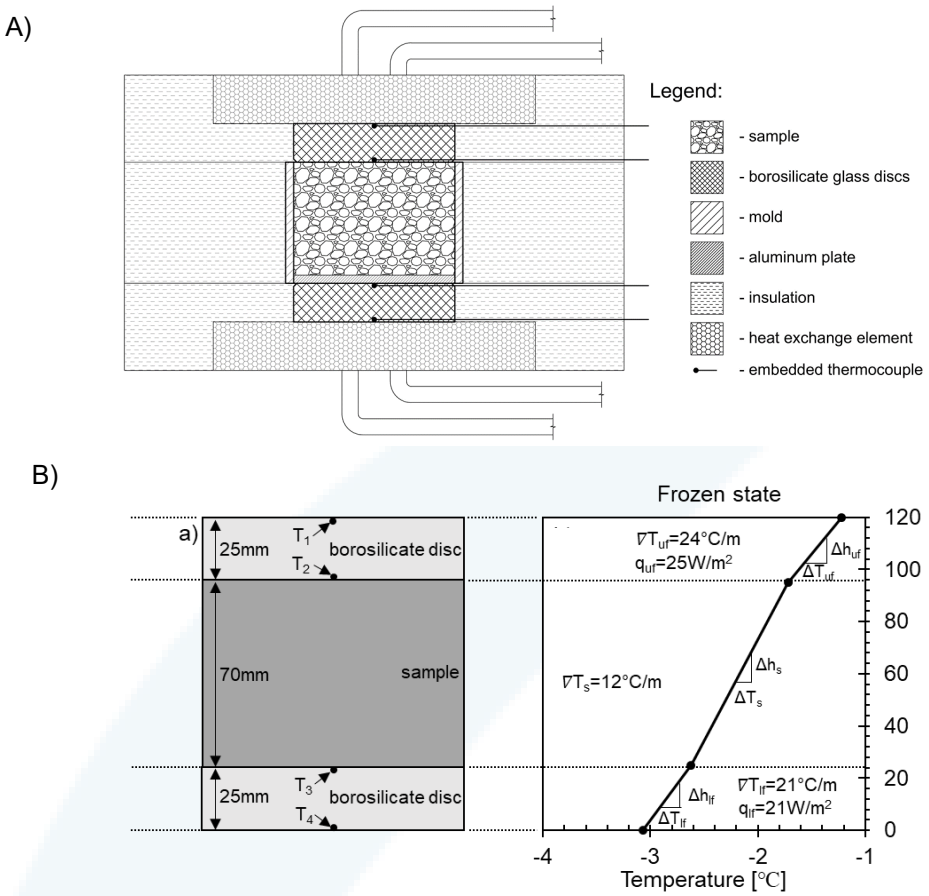

Fig. 6 Thermal conductivity test setup and one measurement example (Lyu, 2021); A) Cross-section of thermal conductivity test setup; B) Thermal conductivity measurement. left: measurement setup sketch, and right: temperature gradient and heat flux through borosilicate discs and sample at Tsoil=(TT+TB)/2=-2.17 ℃.

$$k_T = \frac{q_{uf} + q_{lf}}{2} \cdot \frac{h_s}{\left(T_A - T_B\right)} \tag{6}$$

where q_{uf} and q_{lf} are the heat fluxes through the upper and lower glass discs, respectively, h_s is the height of the sample, TT and TB are the temperatures at the top and bottom of the sample, respectively. Given that k_T is temperature-dependent, TT and TB were meticulously controlled to maintain a consistent difference of $\Delta T_s = 1$ ºC ensuring precise and reliable results. An exemplary set of test results, obtained at $T_{soil} = \frac{TT + TB}{2} = -2.17$ ºC, is given in Fig. 6-B.

4.2.1 Test results

Fig. 7 illustrates the outcomes of the thermal conductivity tests conducted on the remoulded soils. An abrupt rise in k_T was observed upon the initiation of ice crystallization, followed by a gradual increase as freezing progressed. This behaviour is indicative of the enhanced thermal conductivity of ice in comparison to water. To consider the varying saturation and properties of the top 3 m sand layer, two parameters are adjusted: one for the top 0.7 m, referred to as “sand1”, and another for the remaining part of the layer, referred to as “sand2”.

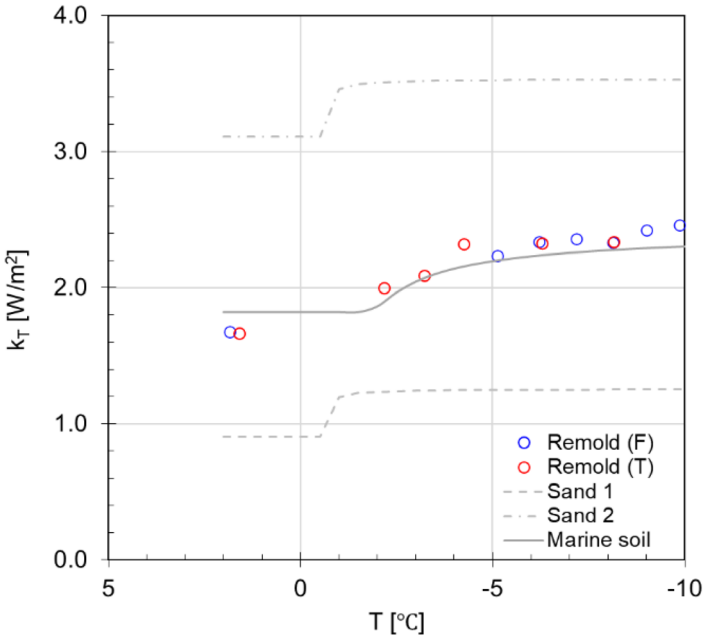

Fig. 7 Measured and adopted k_T vs. T relations (Lyu, 2021). Remold (F) and Remold (T) represent measured results in the process of freezing and thawing, respectively, for the marine clay layer. Sand1 and Sand2 stand for the sand layer in the top 0.7 m, and the sand layer from 0.7 to 3 m depth, respectively.

4.3 Undrained creep tests

The creep tests were conducted using a temperature-controlled triaxial setup, as shown in Fig. 8. To minimize potential disruptions from frozen soil during installation and enhance temperature control, the entire apparatus was positioned within a temperature-controlled cold room with fluctuations limited to ±2°C. Thermal H5, an anti-freeze refrigerant designed for a working temperature range of -50~+105°C, was used for the confining and temperature-controlled fluid inside the triaxial cell. The control of cell temperature was achieved by employing a refrigerated circulator to circulate Thermal H5 through a spiral copper coil within the cell. The temperature of the circulating fluid was continuously adjusted based on the variance between the target temperature and the reading of a thermocouple located 30 mm away from the sample. This combination of temperature feedback control and a double insulation layer allowed to maintain an impressive accuracy of ±0.02°C.

The setup features a high-resolution loading frame capable of constant-strain rate or constant-stress loading tests. An LVDT with a 50 mm measuring range and ±0.01 mm accuracy was attached to the loading rod to measure axial displacement. The top cap was specially designed to ensure precise point-plane contact with the loading rod. Two piston pumps were employed to control both the cell and back pressure. Notably, the cell pressure pump used the same Thermal H5 refrigerant as the triaxial apparatus and the refrigerated circulator, ensuring consistency in thermal performance.

The creep tests were run without pore pressure measurement since anti-freezing liquid could cause more disturbance on samples during longer running time in creep tests. All tests were carried out at a constant confining stress of 100 kPa, with variations in testing temperature (-3 & -5°C) and deviatoric stress levels (200 ~ 1500 kPa). The tests are listed in Table 1.

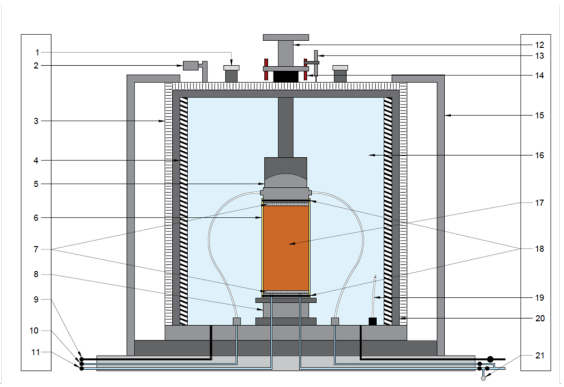

1 Fluid Circulation Valve	8 Bottom Pedestal	15 Metal Insulation Panel
2 Air Valve	9 Cell Valve	16 Cell Fluid
3 Cell Wall Insulation	10 Bottom Cap Valve	17 Test Sample
4 Coil	11 Top Cap Valve	18 O-ring
5 Top Cap	12 Loading Rod	19 Thermometer
6 Rubber Membrane	13 Local LVDT	20 Cell wall
7 Porous Stone	14 Plastic Cylinder	21 Pore Pressure Sensor

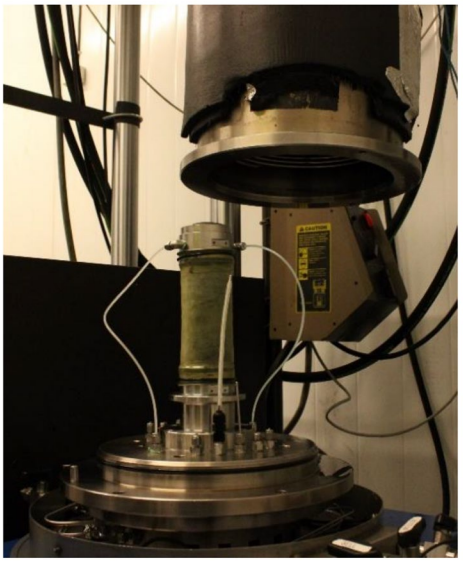

Fig. 8 Triaxial setup sketch (left) and the built-up sample on the triaxial pedestal (right)

Table 1 List of creep tests on Longyearbyen clay samples

Test no.	Depth	T [°C]	S [g/L]	wc [%]	σ_3 [kPa]	q [kPa]
i-1	4.2~4.6 m	-3	24	22.3	100	191
i-2	4.2~4.6 m	-3	26	22	100	248
i-3	4.2~4.6 m	-3	25	22.2	100	345
i-4	4.6~5.0 m	-3	27	20.9	100	450
i-5	4.6~5.0 m	-5	24	19.5	100	273
i-6	4.6~5.0 m	-5	25	20.2	100	364
i-7	4.6~5.0 m	-5	24	19.9	100	490
i-8	4.6~5.0 m	-5	25	23	100	558
i-9	4.2~4.6 m	-5	21	21.9	100	728
i-10	4.6~5.0 m	-5	30	20	100	1450

T: temperature, S: salinity, wc: gravimetric water content, σ_3: cell pressure, q: deviatoric stress.

4.3.1 Test results

All tests exhibited immediate deformation followed by significant time-dependent deformation, with distinct creep stages (primary, secondary, and tertiary). The rate of deformation and creep were observed to be contingent on both deviatoric stress and temperature. These findings align with earlier laboratory tests on various frozen soils and permafrost, as demonstrated in (*Arenson and Springman*, 2005). Test results are given in Fig. 9.

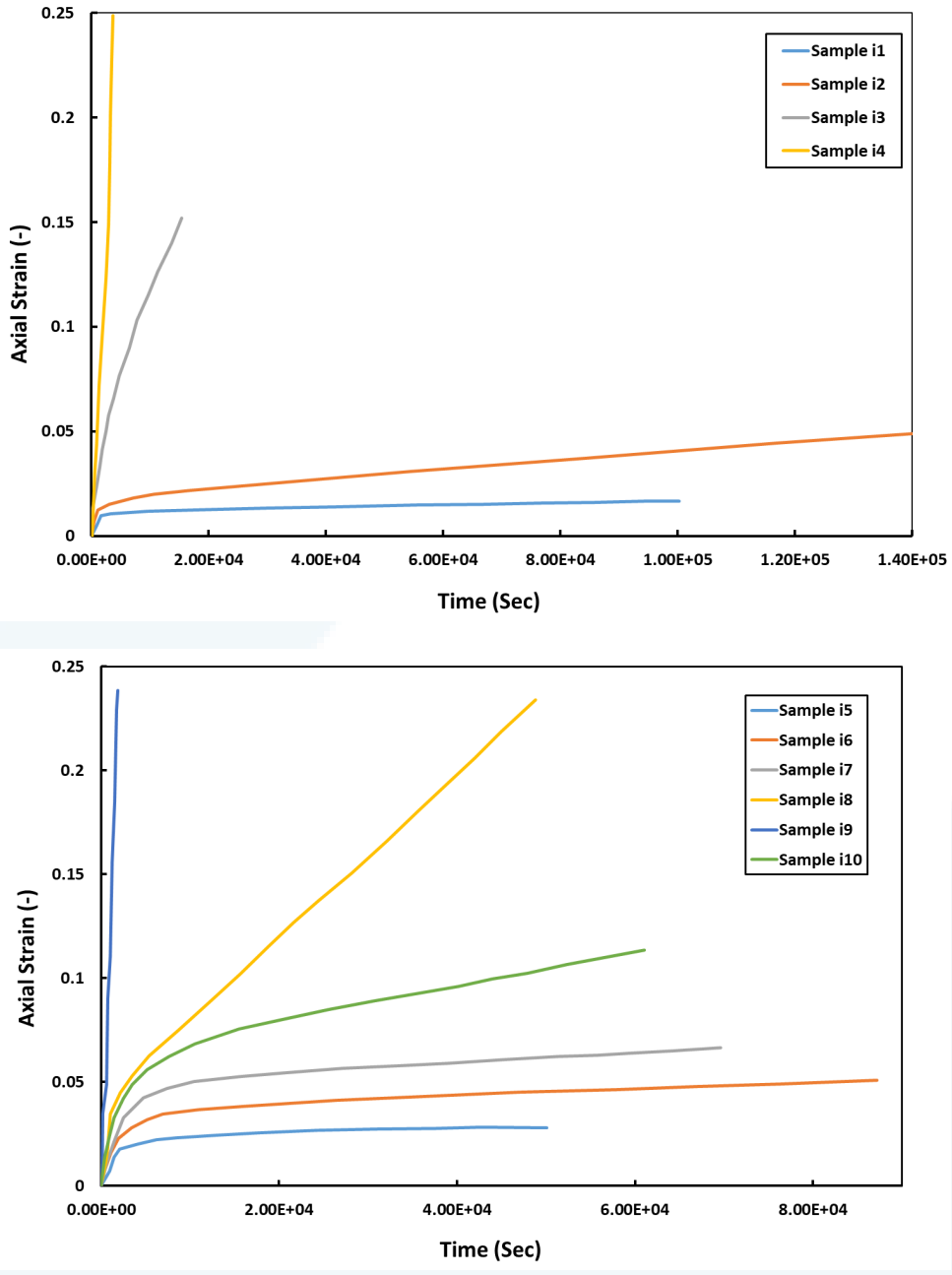

Fig. 9 Creep test results (Lyu, 2021)

5 Plate loading test

The plate load test is typically a field test used to determine the ultimate bearing capacity of the foundation and its potential settlement under a specific load. In this case, the primary focus was on long-term settlement in response to temperature changes, rather than ultimate capacity. To ensure that the plate (foundation) remained below the active layer, which has an approximate depth of 1~2 meters, as is common practice in permafrost regions, the foundation depth was set at 3.5 ~ 4 meters. This depth aligns with the location of the frozen saline clay of marine sediment origin, the main area of interest in this project, which is typically found below 3 ~ 4 meters based on borehole drilling and electrical resistivity tomography data. To achieve this depth and properly load the plate, a pile was used to support the foundation. The optimal foundation depth was determined as 4.2 meters, with a pile extending approximately 0.8 meters above the ground surface.

The plate settlement might influence to a large extent by anomaly (e.g. gravels and ice blocks) when anomaly size is comparable with plate dimension. According to the investigation reported by *Gilbert et al.* (2019) no gravel-sized anomaly or ice blocks were found in the layer of silty clay (marine deposit), and the layer is quite homogeneous with weakly laminated mud. Considering available size of drilling rig, the 280 mm diameter plate was selected for the test.

Several challenges were encountered during the construction and installation of the test setup. First, conducting field tests in permafrost regions presents a significant financial challenge due to the high costs associated with human resources, transportation, and materials. For instance, the initial design involved a hollow concrete column to install an extensometer for measuring vertical displacement variations beneath the footing. However, casting concrete piles/columns is only possible on the Norwegian mainland, and transporting them to Longyearbyen substantially would inflate the budget. Consequently, locally available wooden piles were chosen, necessitating the abandonment of the extensometer idea.

The test setup is exposed to extreme weather conditions, and the permafrost is highly sensitive to thermal disturbances caused by both the construction process and the necessary infrastructure. Therefore, evaluating sensor configurations is crucial. Additionally, construction must take place during subzero temperatures, preferably in late fall or winter, to minimize the impact of the construction phase. It is essential to prevent the permafrost from thawing due to warm air temperatures and construction-related heat. The measurements indicated that it took several months for the ground temperature to return to its original field condition due to the inevitable thermal disturbance during construction. To mitigate this, wooden or concrete piles are favoured over steel piles, as the latter conducts heat efficiently. A tent shelter was placed over the steel frame, and the loading platform to prevent sun radiation absorption during summer.

This test is mainly to study time-dependent settlement, with focus of end bearing. However, the infrastructure in permafrost is normally subject to far more complicated state of stress, such as heaving stress with active layer freezing and ad-freeze bonding between piles and the ground. Finally, casings were adopted to maintain the borehole and left enough space between casings and piles. All efforts assure the equality between loading force and end-bearing force, eliminates the contribution of side friction. The wooden piles are waxed with grease and wrapped in bubble plastic to prevent ad-freeze bounds of water and ice. Thermal insulation is installed around the pile at the surface to decrease the heat exchange from air convection and to maintain the natural temperature conditions of the soil. Air convection is not a big problem during summer, as the warmer air will stay at the surface. However, in winter, cold air might flow down the air gap between the pile and casing, influencing the thermal regime. The wooden pile, footing, and casing are illustrated in Fig. 10.

Fig. 11 provides an illustration of the experimental setup. It involves three predrilled holes with a diameter of approximately 320 mm for the piles. Each hole contains a base layer of about two liters of dry sand. A circular steel footing plate with a diameter of 280 mm is affixed to the bottom of the wooden pile. At the top of the pile, an equivalent 300 mm steel plate is attached.

Fig. 10 Pile installation

A steel framework was meticulously crafted atop the pile, interconnecting these piles into a rigid foundation for the accompanying concrete slabs. This setup ensures an even distribution of the load across the piles. Fig. 12 provides an insightful depiction of the plate loading test frame. Load cells affixed to the apex of each pile carefully gauge the precise magnitude of the load exerted on each pile. Vertical displacements were diligently tracked through a wire sensor positioned between the wooden pile and the frozen steel casing anchored beneath the pile. To maintain a reference point for measurements, an inert steel bar has been securely positioned at a depth of 5.5 meters beneath the ground, in close proximity to the three piles, as illustrated in Fig. 13. These movements are also cross-referenced with the nearby UNIS building. Additionally, temperature sensors were stationed at every footing plate. In preparation for data logging throughout both winter and summer, a compact wind turbine and solar panel have been thoughtfully installed to ensure a consistent power supply.

The testing commenced in May 2020, initially bearing the load of two substantial concrete slabs, each weighing 1400 kg. This load was incrementally augmented, accommodating 4, 6, 9, and eventually 12 slabs in October 2020, March 2021, July 2021, and February 2022, respectively. For a visual insight into the final stages of the plate loading test, refer to Fig. 12. The image vividly showcases the steel frame and the imposing concrete slabs. It is noteworthy that the wooden piles, integrated to the test's structure, are deliberately hidden beneath the green tarpaulin. This measure has been taken to eliminate potential heat transfer, ensuring the test's accuracy and reliability.

The test setup and procedure can be summarised as (*Lyu*, 2021):

1- Three $\phi = 320$ mm holes have been bored through the active layer and sandy permafrost down to the clay permafrost.

2- Wooden columns are standing at circular footing plates 4.2 m down in the ground, carrying load only at their tip.

3- Casing supports the soil around the boreholes, provides an air gap along the shaft of the piles and prevents leakage of surface water to the columns.

4- Load cells at the top of each pile measures the actual weight loaded to on each wooden column.

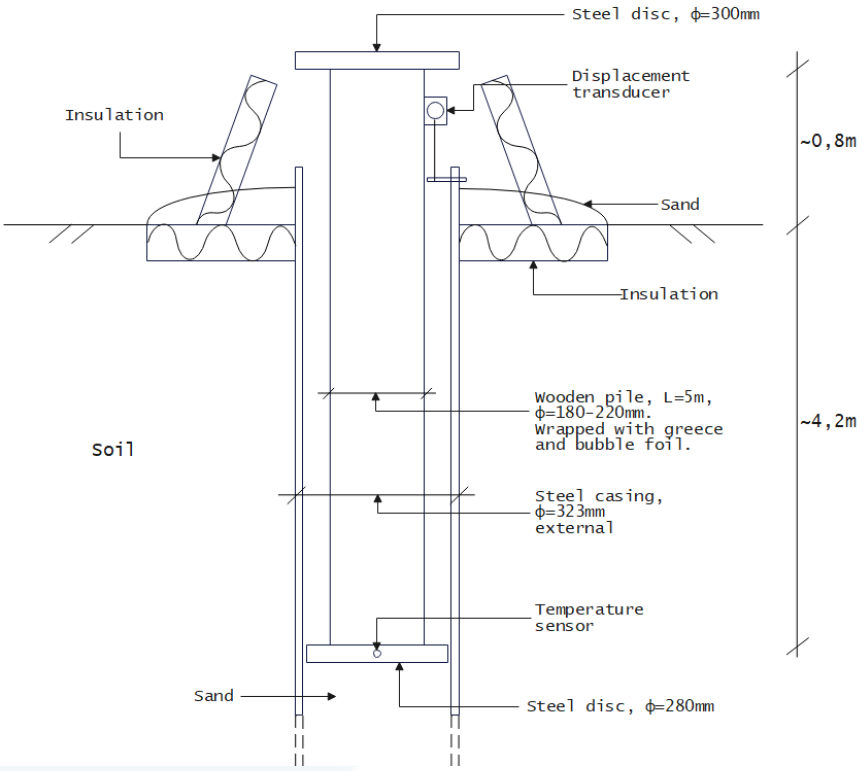

Fig. 11 Illustrated profile of the plate loading test (Farnes, 2023)

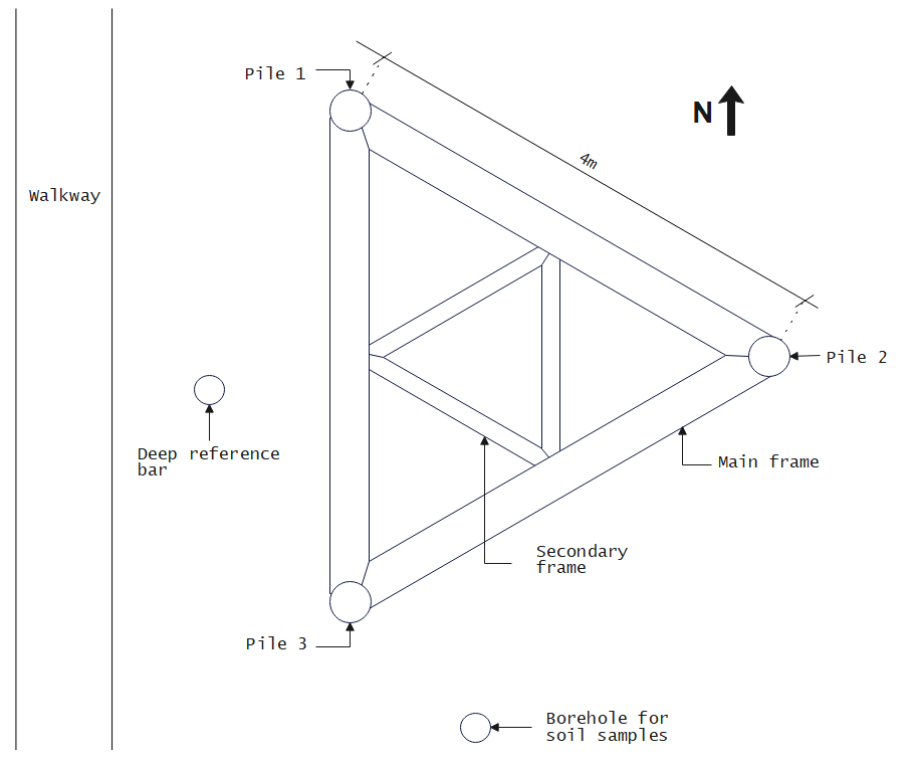

Fig. 12 Illustrated overview of the plate loading test frame (Farnes, 2023)

5- Vertical displacements are monitored by a wire displacement sensor between each column and the steel pipe casing that is frozenly bounded to the soil. An unloaded steel bar is fixed 5.5 m down in the ground for reference and checking vertical movements. Movements are also checked against the UNIS building.

6- Temperature sensors are placed at each footing plate.

7- Thermal insulation around the pile at the surface prevents unintended heat leak into the soil, aiming to maintain the natural temperature conditions in the soil.

8- Annual temperature at 4.2 m depth varies from -2.5ºC to -3.2ºC through the year. As summer heat takes time to penetrate the frozen soil, the warmest month is February, and the coldest month is May at the site.

9- As loading blocks, concrete slabs with weight of 1400 kg each are used. The dead weight started from 2 blocks in May 2020, and went up to 4, 6, 9 and 12 blocks in October 2020, March 2021, July 2021 and February 2022, respectively.

Fig. 13 Loading blocks configurations at different stages

5.1 Test results

Ground temperature monitoring has been diligently conducted from the surface to a depth of 30 meters, using the thermistors positioned near the test site. This comprehensive record spans from late September 2018 onwards and is located at point E5, as depicted in Fig. 14. The gathered surface temperature data, as displayed in Fig. 15, is accompanied by an estimated sinusoidal function eliminating temperature fluctuation. This function was derived through a least square method to optimize its fit to the temperature data. It is worth noting that the data sensor

encountered some measurement issues, leading to intermittent gaps in the dataset. This issue was especially pronounced in 2021, as evident in the figure.

The ground temperature profile on the first day of loading is recorded from the nearby thermistor E5 and presented in Fig. 16. The temperature profile at the end of first spring, summer, fall, and winter is presented in Fig. 17. These are also recorded from E5 thermistor.

Fig. 14 Positions of the temperature monitoring borehole and the test site (Farnes, 2023)

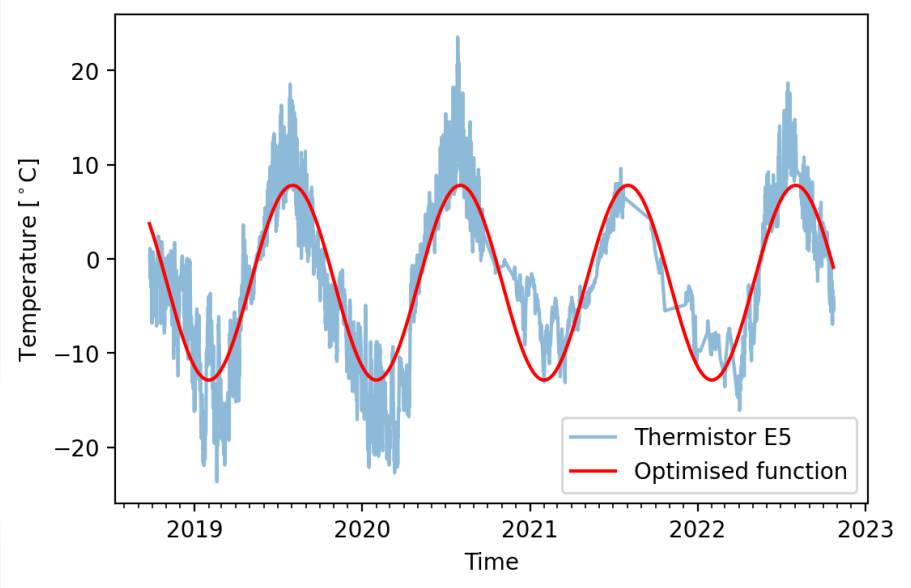

Fig. 15 Measured surface temperature of thermistor E5 along with an optimized sinusoidal function of the temperature.

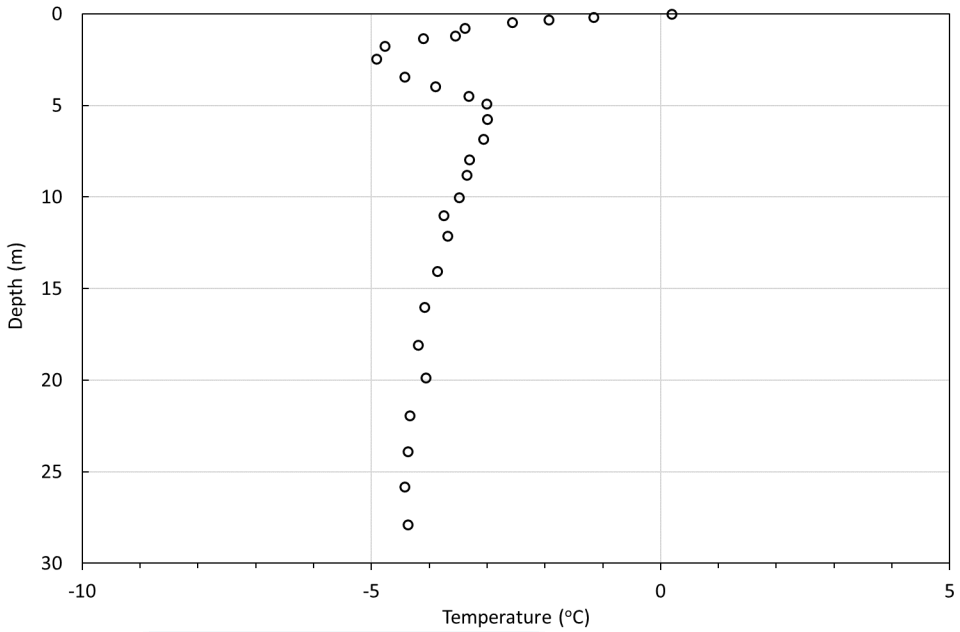

Fig. 16 Profile of the ground temperature at thermistor E5 on the first day of loading

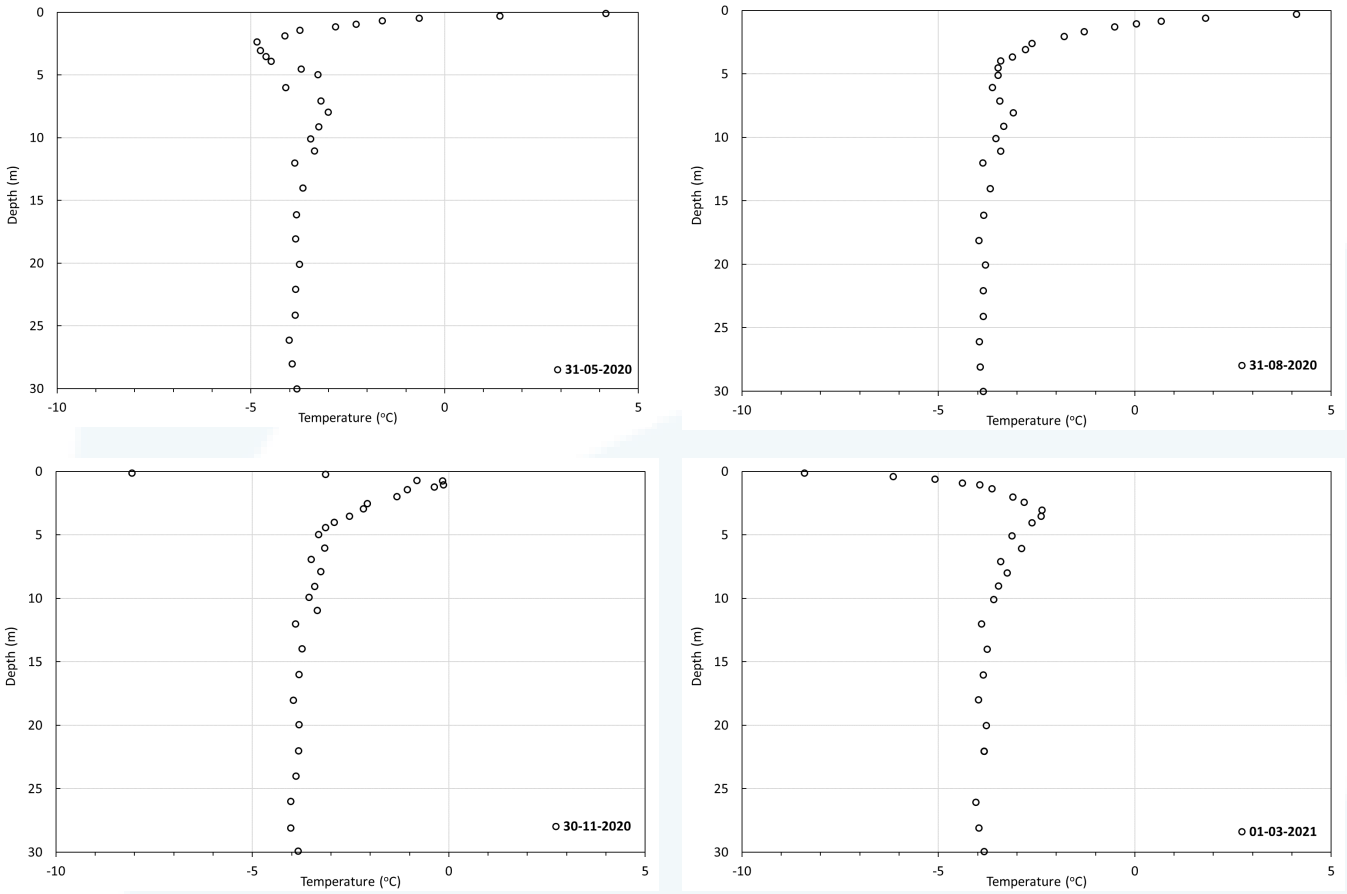

Fig. 17 Temperature profile at the end of first spring, summer, fall and winter

Temperature at the pile tips were recorded during the test period. Two thermistors of lesser accuracy, denoted as T2, were affixed at the bases of pile 1 and pile 2. These T2 thermistors commenced their measurements in mid-May 2020. Then, in July 2020, three carefully calibrated thermistors, labelled as T1, were meticulously installed, reaching down to the bottom of column 1 through 3. The installation process involved the use of plastic pipes, which had been pre-attached to the columns back in March 2020. The recording of both sets is illustrated in Fig. 18.

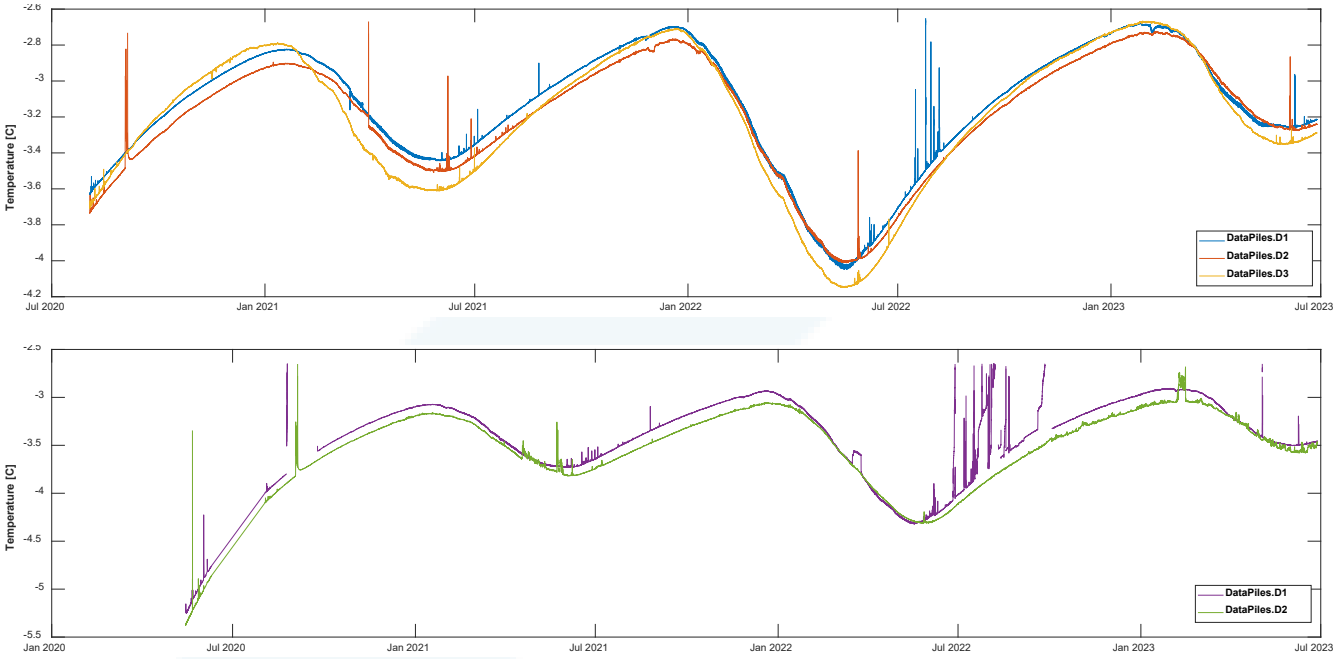

Fig. 18 Temperature record at pile tips; top) T1 thermistors set; bottom) T2 thermistors set

The plates experienced five stepwise loading events. Initially, in mid-May 2020, two concrete blocks (2.8 tons) were placed. However, the recording system was initiated a week later, resulting in the lack of instant settlement data for the first loading event in the dataset presented in Fig. 19.

The second loading event occurred at the end of October 2020 when two more concrete blocks were added, bringing the total load to 5.6 tons. In the third loading event in March 2021, all previous loads (four blocks) were first removed, and then a dead weight of six blocks was reintroduced after 24 hours. Notably, a rebound of approximately 1 to 2 mm and a faster settlement after the application of the heavier dead weight were observed.

Following observations can be highlighted from the tests:

1- While T2 sensors are less accurate, they consistently exhibit an offset of around 0.35°C compared to the well-calibrated sensors, T1. The data from T2 suggests that the construction event, which took place during the winter of 2020, led to further cooling of the studied permafrost, reducing the temperature from approximately -3.1±0.3°C to below -5°C. It's noteworthy that this thermal disturbance required 3 to 4 months to gradually return to the original temperature prior to the construction.

2- A delay in temperature fluctuations from the surface (Fig. 15) to the pile tips (Fig. 18) is observed. The surface temperature has a maximum and minimum in July and February, respectively, while the pile tips temperature has a maximum and minimum in February and May/June, respectively.

3- Uplifting was not observed, indirectly indicating the disconnection between the columns and the casings.

4- The settlement rate was observed to depend on both temperature and load level. An immediate increase in plate displacement followed whenever the external load was raised. Additionally, it was noted that as the temperature approached the maximum, approximately around -3°C, the creep rate increased, typically occurring around December each year.

5- The thawing/freezing temperature of the marine clay layer was determined to be around -1.6°C, influenced by its salt content. As shown in Fig. 5, when the soil temperature approached the thawing temperature, the unfrozen water content rapidly increased, which resulted in an increase in the creep rate.

6- The uneven settlement of the three plates could be attributed to slight differences in embedment depth and potential variability in the mechanical properties of the frozen soil. However, the significant variation in instantaneous displacement observed after the second loading event on October 28, 2020, might suggest a measurement error for Pile 2.

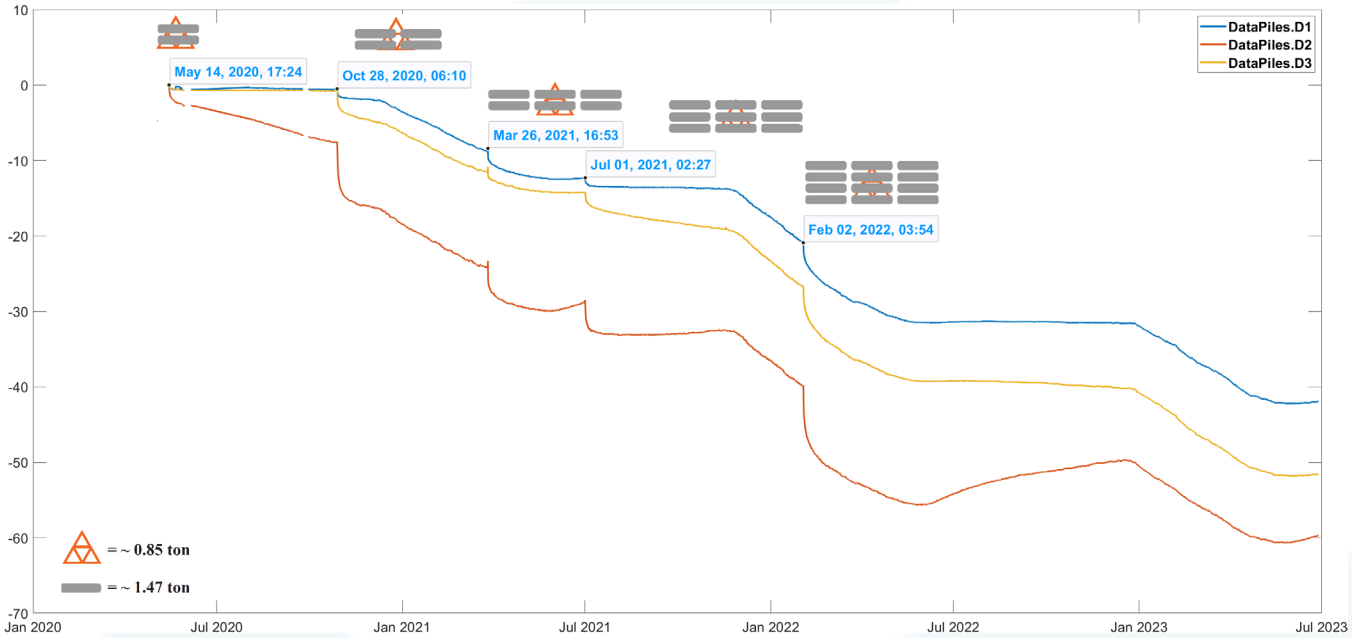

Fig. 19 Plates settlement in time

6 References

Aalto, J., O. Karjalainen, J. Hjort, and M. Luoto (2018), Statistical forecasting of current and future circum-arctic ground temperatures and active layer thickness, *Geophysical Research Letters*, *45*(10), 4889-4898.
Arenson, L. U., and S. M. Springman (2005), Triaxial constant stress and constant strain rate tests on ice-rich permafrost samples, *Canadian Geotechnical Journal*, *42*(2), 412-430.
Biskaborn, B. K., S. L. Smith, J. Noetzli, H. Matthes, G. Vieira, D. A. Streletskiy, P. Schoeneich, V. E. Romanovsky, A. G. Lewkowicz, and A. Abramov (2019), Permafrost is warming at a global scale, *Nature communications*, *10*(1), 1-11.
Doré, G., F. Niu, and H. Brooks (2016), Adaptation methods for transportation infrastructure built on degrading permafrost, *Permafrost and Periglacial Processes*, *27*(4), 352-364.
Duvillard, P.-A., L. Ravanel, M. Marcer, and P. Schoeneich (2019), Recent evolution of damage to infrastructure on permafrost in the french alps, *Regional Environmental Change*, *19*(5), 1281-1293.
Eckardt, H. (1979), Creep behaviour of frozen soils in uniaxial compression tests, *Engineering Geology*, *13*(1), 185-195.
Etzelmüller, B., T. V. Schuler, K. Isaksen, H. H. Christiansen, H. Farbrot, and R. Benestad (2011), Modeling the temperature evolution of svalbard permafrost during the 20th and 21st century, *The Cryosphere*, *5*(1), 67-79.

Farnes, H. T. (2023), Pile loading test in permafrost: Back analysis of settlements using an elasto-viscoplastic model, MSc Thesis, Norwegian University of Science and Technology.
Ghoreishian Amiri, S. A., G. Grimstad, and M. Kadivar (2022), An elastic-viscoplastic model for saturated frozen soils, *European Journal of Environmental and Civil Engineering*, *26*(7), 2537-2553.
Gilbert, G. L., A. Instanes, A. O. Sinitsyn, and A. Aalberg (2019), Characterization of two sites for geotechnical testing in permafrost: Longyearbyen, svalbard [j], *AIMS Geosciences*, *5*(4), 868-885.
Gilbert , G. L., I. Arne, O. S. Anatoly, and A. Arne (2019), Characterization of two sites for geotechnical testing in permafrost: Longyearbyen, svalbard, *AIMS Geosciences*, *5*(4), 868-885.
Instanes, A. (2016), Incorporating climate warming scenarios in coastal permafrost engineering design – case studies from svalbard and northwest russia, *Cold Regions Science and Technology*, *131*, 76-87.
Karijord, C. (2018), Råte truer husene på svalbard, in *High North News*, edited.
Keller, G. V., and F. C. Frischknecht (1966), *Electrical methods in geophysical prospecting*.
Luhn, A. (2016), Slow-motion wrecks: How thawing permafrost is destroying arctic cities, in *The Guardian*, edited.
Lyu, C. (2021), Mechanical behavior of frozen saline clay: Laboratory, field and numerical investigation, PhD Dissertation, Norwegian University of Science and Technology (NTNU).
Lyu, C., S. A. G. Amiri, G. Grimstad, K. V. Høyland, and T. Ingeman-Nielsen (2020), Comparison of geoacoustic models for unfrozen water content estimation, *Journal of Geophysical Research: Solid Earth*, *125*(10), e2020JB019766.
Oldenborger, G. A., and A.-M. LeBlanc (2018), Monitoring changes in unfrozen water content with electrical resistivity surveys in cold continuous permafrost, *Geophysical Journal International*, *215*(2), 965-977.
OSBORNE, H. (2018), Arctic permafrost thaw will start toppling buildings across northern hemisphere by 2050, in *Newsweek*, edited.
Osterkamp, T. (2007), Characteristics of the recent warming of permafrost in alaska, *Journal of Geophysical Research: Earth Surface*, *112*(F2).
Wu, Q., and T. Zhang (2008), Recent permafrost warming on the qinghai-tibetan plateau, *Journal of Geophysical Research: Atmospheres*, *113*(D13).